

FROM FIRE OBSERVATIONS TO SMOKE PLUME FORECASTING IN THE MACC SERVICES

Johannes W. Kaiser¹, A. Benedetti¹, J. Flemming¹, J.-J. Morcrette¹, A. Heil², M. G. Schultz², G. R. van der Werf³, and M. J. Wooster⁴

¹European Centre for Medium-range Weather Forecasts, United Kingdom

²Forschungszentrum Jülich, Germany

³Free University of Amsterdam, The Netherlands

⁴King's College London, United Kingdom

ABSTRACT

The MACC project is implementing atmospheric monitoring and forecasting services for the global and European domains as part of the GMES programme. Smoke plumes are monitored by assimilating observations of aerosol optical depth and various trace gases. Biomass burning is monitored in real time by assimilating observations of fire radiative power (FRP) from five satellite-based instruments. The global monitoring capability is demonstrated with a near real time fire and smoke analysis for South America, where a threefold increase of biomass burning has been detected in 2010 compared to 2009. Furthermore, an anomalously flat diurnal cycle has been recorded for the Russian wildfires of July and August 2010. This can be interpreted as a characteristic of peaty soil burning, which entails particularly large emissions. The global aerosol service was able to forecast, with three days lead time, an air quality threshold transgression in Finland that resulted from the Russian fires.

Key words: fire emissions, fire radiative power, FRP, GMES, MACC, aerosol optical depth, AOD, peat fire, Russia 2010, smoke, air quality forecast.

1. INTRODUCTION

Monitoring Atmospheric Composition and Climate (MACC) is the current pre-operational atmospheric service of the European GMES programme. MACC provides data records on atmospheric composition for recent years, data for monitoring present conditions and forecasts of the distribution of key constituents for a few days ahead. It combines state-of-the-art atmospheric modelling with Earth observation data to provide information services covering European Air Quality, Global Atmospheric Composition, Climate, and UV and Solar Energy.

The global systems of MACC use an extended version of ECMWF's Integrated Forecasting System (IFS) to as-

simulate satellite-based observations of aerosols, reactive gases and greenhouse gases [e.g. BMB⁺09]. These analyses are produced retrospectively from 2003 to present. Aerosols and reactive gases are also assimilated in near real time for monitoring purposes and to initialise global and regional forecasts of atmospheric composition and air quality [HET⁺08].

While smoke plumes from fires are observed and consequently represented in the analyses, *a priori* information is still required. For example, the relative abundance of the different aerosol types is determined from the aerosol model and not directly adjusted by the assimilation of the MODIS Aerosol Optical Depth (AOD) product [BMB⁺09]. Therefore, and also for continued generation of smoke plumes in the forecast, various species emission fluxes are required by the atmospheric model as surface boundary conditions.

These fluxes must be derived from observations of the actual fire distribution since biomass burning varies strongly on all time scales from hours to decades and beyond [KSG⁺06]. For retrospective analysis, MACC redistributes the GFED3 inventory, which uses burnt area observed by MODIS, [vdWRG⁺10] to 0.1 deg and 1 day resolution using Fire Radiative Power (FRP) observed by MODIS. For real time applications, MACC assimilates FRP from the MODIS [JGK⁺02], SEVIRI [RW08] and GOES-East and -West [XWRF10] instruments, cf. [KSF⁺09].

In this paper, we present the Global Fire Monitoring System (GFAS) developed within MACC for the calculation of smoke emissions from FRP observations. We also show its application for fire and smoke plume monitoring and forecasting of the strong fire seasons in Russia and South America in July–September 2010.

2. FIRE RADIATIVE POWER ASSIMILATION

2.1. Gridding of FRP Observations

The FRP products generally represent the fires observed by the satellite in Watts for each satellite pixel. The assimilation system combines all observations within each of the global grid cells in order to obtain a gridded representation of the satellite observations at one hour resolution.

In practice, no grid cell is observed completely and uniquely during any given one-hour interval: All space-borne observations are restricted by the satellite orbit and observations frequency. No fire product may be produced for sub-grid areas with cloud cover or water bodies. The MODIS product also excludes ice and snow cover. Thus many grid cells are not completely observed. On the other hand, many sub-grid cell areas are observed more than once during one hour due to oversampling of the instruments, the so-called ‘‘butterfly effect’’ of the MODIS scan geometry and the high observation frequency of geostationary satellites.

2.1.1. Input data from the Satellite Products

The MODIS, SEVIRI and GOES fire products provide a mask that identifies observed fire pixels, observed non-fire pixels and pixels for which no fire product was generated, e.g. due to cloud cover. For the fire pixels, the observed fire radiative power F_i and its uncertainty ζ_{F_i} [W] are also listed. For the non-fire pixels $F_i = 0$ and the uncertainty can be approximated by the instrument-specific detection threshold:

$$\zeta_{F_i} = \begin{cases} 10 \text{ MW} & (F_i = 0, \text{MODIS}) \\ 50 \text{ MW} & (F_i = 0, \text{SEVIRI, GOES}) \end{cases} \quad (1)$$

In order to account for additional uncertainties at large view zenith angles θ_i , GFAS uses an adjusted uncertainty

$$\sigma_{F_i} = \frac{\zeta_{F_i}}{\cos(\theta_i)} . \quad (2)$$

This degradation may alternatively be interpreted as counteracting the MODIS butterfly effect. The view zenith angles are taken from auxiliary static data for SEVIRI, the satellite product for GOES, and a fixed parameterisation for MODIS.

The area A_i [m²] and geographical coordinates are also taken from the satellite products, auxiliary data and custom parameterisations. The coordinates are used to assign observed satellite pixels to cells of the global grid.

For each pixel, the FRP density R_i [W m⁻²] and its uncertainty are determined by

$$R_i = \frac{F_i}{A_i} \quad (3)$$

$$\sigma_{R_i} = \frac{\sigma_{F_i}}{A_i} \quad (4)$$

$$= \frac{\zeta_{F_i}}{A_i \cos(\theta_i)} . \quad (5)$$

2.1.2. Upscaling of FRP Density Observations to Global Grid

When each satellite pixel observation is interpreted as independent observation of the entire grid cell’s FRP density ρ , the grid cell’s FRP density and its accuracy can be derived in a consistent way. However, the additional error, due to the fact that each satellite pixel is severely undersampling the grid cell, needs to be taken into account. This is approximated *ad hoc* by degrading each pixel uncertainty σ_{R_i} with the inverse of the root of the observed fraction A_i/a of the grid cell:

$$\rho = \sigma_\rho^2 \sum_i \left(\sqrt{\frac{a}{A_i}} \sigma_{R_i} \right)^{-2} R_i \quad (6)$$

$$= \frac{\sum_i A_i \sigma_{R_i}^{-2} R_i}{\sum_i A_i \sigma_{R_i}^{-2}} \quad (7)$$

$$= \frac{\sum_i A_i^2 \cos^2(\theta_i) \zeta_{F_i}^{-2} F_i}{\sum_i A_i^2 \cos^2(\theta_i) \zeta_{F_i}^{-2} A_i} \quad (8)$$

$$\sigma_\rho^{-2} = \sum_i \left(\sqrt{\frac{a}{A_i}} \sigma_{R_i} \right)^{-2} \quad (9)$$

$$= \frac{1}{a} \sum_i A_i \sigma_{R_i}^{-2} \quad (10)$$

$$= \frac{1}{a} \sum_i A_i^3 \cos^2(\theta_i) \zeta_{F_i}^{-2} , \quad (11)$$

where a denotes the area [m²] of the grid cell and the sum includes all satellite observation pixels i that fall into the grid cell under consideration.

2.1.3. Special Case: Homogeneous Scene and Observation

For homogeneous fires across a grid cell that are observed completely and uniquely with n non-overlapping satellite pixels and $A_i = a/n$, the Eqs. 6–11 simplify to:

$$\rho = \frac{n A \sigma_R^{-2} R}{n A \sigma_R^{-2}} \quad (12)$$

$$= R = \frac{F}{A} \quad (13)$$

$$\sigma_\rho^{-2} = \frac{n}{a} A \sigma_R^{-2} \quad (14)$$

$$= \sigma_R^{-2} = A^2 \cos^2(\theta) \zeta_F^{-2} . \quad (15)$$

These equations imply that the FRP density of the entire grid cell is assumed to be known with the same accuracy

as the one observed in an individual satellite pixel. This demonstrates that the *ad hoc* degradation of each pixel's uncertainty with $\sqrt{\frac{a}{A_i}}$ is a conservative estimate.

2.1.4. Special Case: Observation Error Proportional to Pixel Size

If all FRP density observations are assumed to have an uncertainty $\zeta_{F_i} = A_i$, then Eq. 11 simplifies to

$$\sigma_\rho^{-2} = \sum_i \frac{A_i}{a} \cos^2(\theta_i) . \quad (16)$$

In this case, σ_ρ^{-2} can be interpreted as the average number of observations of all locations within the grid cell for observations near the sub-satellite point with a degradation for large zenith angles. The data presented in this study incorporate this assumption.

2.2. Correction for Water Bodies and Merging of Several Satellites Products

Since it is known *a priori* that only sub-grid cell land areas can burn, the FRP density ρ is corrected with the unitless land fraction δ of the grid cell. Furthermore, gridded FRP observations by several satellites may be merged in a statistically consistent way for an extended temporal window $[t_1, t_2]$. Let $\rho_{j,k}$ denote the FRP density ρ calculated for instrument j in the 1-hour time slot at time t_k . Then the merged FRP density ρ_o with uncertainty ζ_o is calculated as:

$$\rho_o = \zeta_o^2 \sum_{j,k} (c_j \delta \sigma_{j,k})^{-2} c_j \delta \rho_{j,k} \quad (17)$$

$$\zeta_o^{-2} = \sum_{j,k} (c_j \delta \sigma_{j,k})^{-2} , \quad (18)$$

where the sums run over all indices j in the set of considered instruments and all k with $t_k \in [t_1, t_2]$, and where c_j is an instrument-specific bias correction factor. For the daytime and nighttime observations presented in Section 5 below, the time periods are set to the appropriate 12-hour intervals. For all other presented data, they are set to a 24-hour interval and the resulting FRP values are interpreted as daily average values, assuming that the diurnal cycle of the fires is reasonably well sampled by the observations. The approach thus avoids making *ad hoc* assumptions on the diurnal cycle of the fires.

The achieved global sampling is illustrated in Fig. 1, which shows ζ_o^{-2} for the 24-hour interval of 00–24 UTC on 1 October 2010, separately for each of the five available satellite instruments. The SEVIRI observations over South America are excluded because of doubt about their reliability. The geostationary satellites sample the diurnal

cycle very well. Combining the two MODIS instruments also achieves a reasonable sampling frequency, even if the plotted fields still incorporate oversampling by about a factor two. The fire data presented in this study take only SEVIRI and the two MODIS instruments into account. The merged global distribution of FRP density ρ_o according to these three instruments and Eq. 17 is illustrated in Fig. 2.

3. CONVERSION OF FIRE RADIATIVE POWER TO SPECIES EMISSIONS

The fire emission flux density f_s [$\text{kg s}^{-1} \text{m}^{-2}$] of any species s is approximately proportional to the FRP. It is therefore calculated as

$$f_s = \rho_o \times \alpha \times \beta_s , \quad (19)$$

where the units of α are kg J^{-1} , $\rho \times \alpha$ is the combustion rate density [$\text{kg}(\text{dry matter}) \text{s}^{-1} \text{m}^{-2}$], and β_s are biome-dependent emission factors [$\text{kg}(\text{species } s) \text{kg}^{-1}(\text{dry matter})$] [WRPK05, IK05].

We use emission factors β_s from the GFEDv2 inventory [vdWRG⁺06, AM01], which distinguish between the three land cover classes “savanna”, “tropical forest” and “other forest”. The geographical land cover map is derived from the MODIS land cover classification.

Based on a comparison with GFEDv2, $\alpha = 1.37 \cdot 10^{-6} \text{ kg}(\text{dry matter}) \text{J}^{-1}$ has been chosen for the current real time system GFAS0 [KFS⁺09]. The upcoming version will use land cover-specific values [HKvdW⁺10].

4. SOUTH AMERICA IN 2010

The average monthly FRP observed by MODIS since 2003 over Southern Hemisphere America and processed by GFAS is depicted in Fig. 3. The signal is dominated by biomass burning in the Amazon. It appears to display a negative trend since years 2005 that is overlaid by two very strong fire seasons in 2007 and 2010. The trend may be hinting at reduced deforestation. A comparison with the El Nino index shown in Fig. 4 reveals that the two strong fire seasons coincide with strong transitions of El Nino to La Nina regimes.

The fire observations show an increase of fire activity by about a factor of three since 2009. Comparison with smoke aerosol observations over the Amazon may be used to verify this finding. Fig. 5 compares the AOD observed in September 2009 and 2010 over the AERONET station in Ji Parana [HSE⁺01]. They show an increase by a factor of about three. Since aerosols in this location are dominated by smoke this confirms any conclusions drawn from the fire observations in GFAS. The figure also shows the AOD of the MACC real time analysis. Its absolute values as well as day-to-day variations agree well

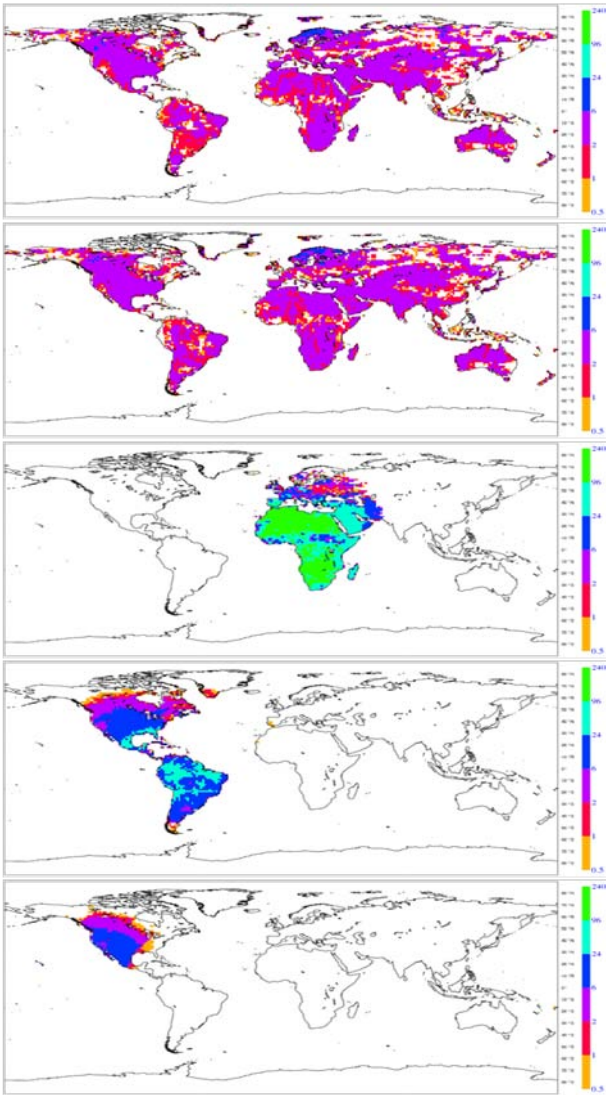


Figure 1. Average number of observations of all locations within the grid cells on 1 October 2010 by MODIS on Terra and Aqua, SEVIRI and GOES-East and -West (top to bottom). Multiple observations, e.g. due to over-sampling, and an artificially superimposed degradation for large viewing angles are included.

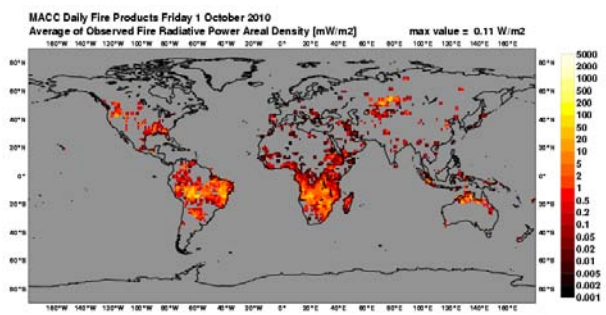


Figure 2. Daily average Fire Radiative Power (FRP) density [$mW m^{-2}$] observed by SEVIRI and the two MODIS instruments on 1 October 2010 and published on the MACC web pages on 2 October 2010.

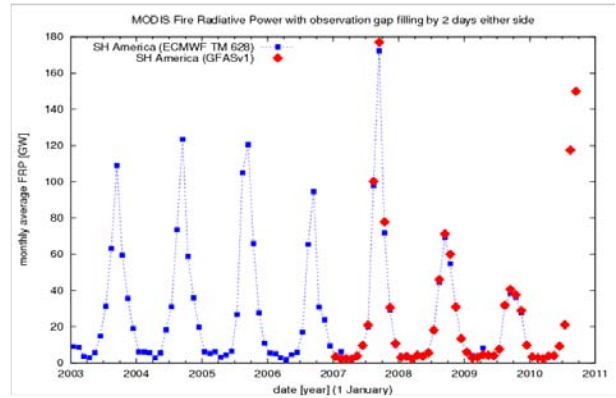


Figure 3. Monthly Fire Radiative Power observed over Southern Hemisphere South America during January 2003 – September 2010. The different symbols denote different spatial resolutions during the gridding.

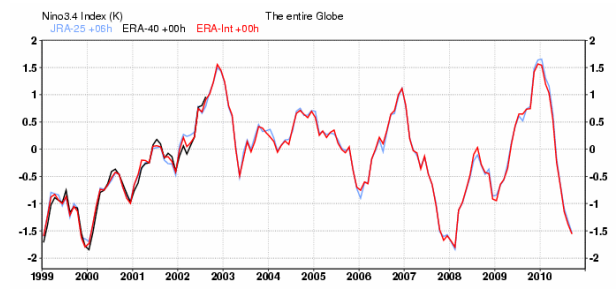


Figure 4. El Nino index from meteorological reanalyses for 1999–2010, ERA Interim in red. (courtesy P. Berrisford)

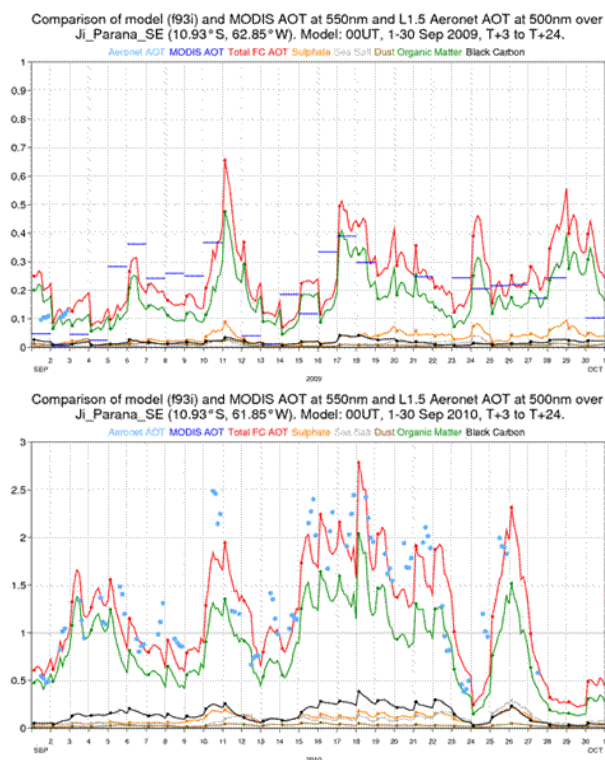


Figure 5. Observed (blue) and modelled (red) aerosol optical depth over Ji Parana, Amazon, in September 2009 (top) and 2010 (bottom). Dark blue observation lines are daily MODIS AOD data, light blue symbols are AERONET observations. The red line represents the MACC aerosol analysis, and the green and black lines are the contributions organic matter and black carbon, respectively, i.e. smoke. Note the different scales of the plots. (graphics by L. Jones)

with the observations. We attribute this quality to a combination of the assimilation of MODIS AOD, excellent representation of atmospheric transport in IFS and up-to-date fire emission input.

5. RUSSIA IN SUMMER 2010

Following anomalously high temperatures, large wildfires devastated parts of Russia to the east of Moscow in July and August 2010, cf. Fig. 6. Because of the dry conditions, peaty soil fires developed, which emitted large quantities of smoke. The thermal radiation of the fires and the aerosol optical depth of the smoke were observed by NASA's MODIS instruments and used in the global real time forecasting system of MACC. Fig. 7 shows the distributions of fires on 4 August and of smoke on 8 August as represented in MACC. The time series of in-situ observations of PM10 in Fig. 8 show that the air quality of Virolahti in Finland was affected by smoke around 8 August, which caused a transgression of the EU threshold of $50 \mu\text{g}(\text{PM}_{10}) \text{m}^{-3}$ for the 24-hour average. The 1-day and 3-day forecasts of PM10 at Virolahti that were

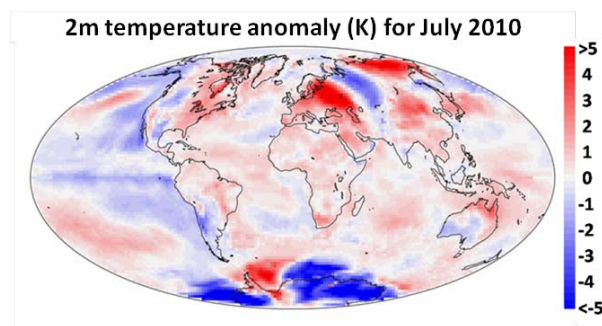


Figure 6. Global 2 m temperature anomaly [K] in July 2010. (data: ERA Interim, graphics: A. Simmons)

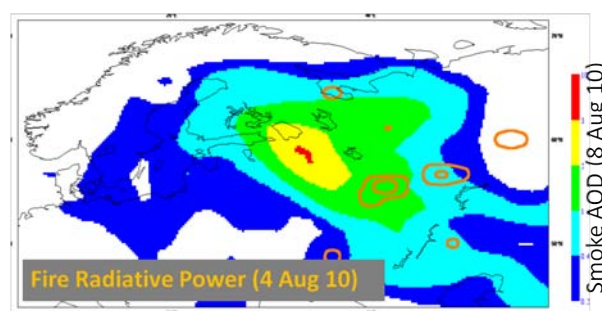


Figure 7. Smoke and fires in Russia in summer 2010 as represented in the global MACC system: Aerosol optical depth of anthropogenic aerosols in the 1-day forecast extending to Finland on 8 August 2010 (colour-coded) and observed fires four days before (FRP contour lines at 50 and 500 mW m^{-2} fire radiative power).

produced by the global MACC system match the in-situ observations well, thus highlighting the ability of MACC to monitor and forecast the global distribution of aerosols with an accuracy that allows local air quality applications. The excellent accuracy is primarily attributed to the combination of data assimilation of aerosol optical depth observations with the accurate representation of atmospheric transport in the IFS.

The observed FRP over the wildfire region East of Moscow is plotted separately for daytime and nighttime in Fig. 9. The multi-annual time series shows two distinct fire seasons in spring (presumably agricultural waste burning) and summer. The time series show that the daytime fire radiative energy release of the wildfires in 2010 was comparable to that of previous years. However, the fires were unique in so far as they burnt with undiminished intensity throughout night, while the fires during the previous years appear to extinguish virtually completely at nighttime. The time series of daily observed FRP clearly displays this flat diurnal cycle for the extreme fire episode from 25 July to 15 August. This fire behaviour can be understood if the fires are mostly “peaty soil fires”, which agrees with public media reports. Emissions from such fires need to be characterised with different conversion factors α and emission factors β_s than those from forest or agricultural fires. Thus the observing

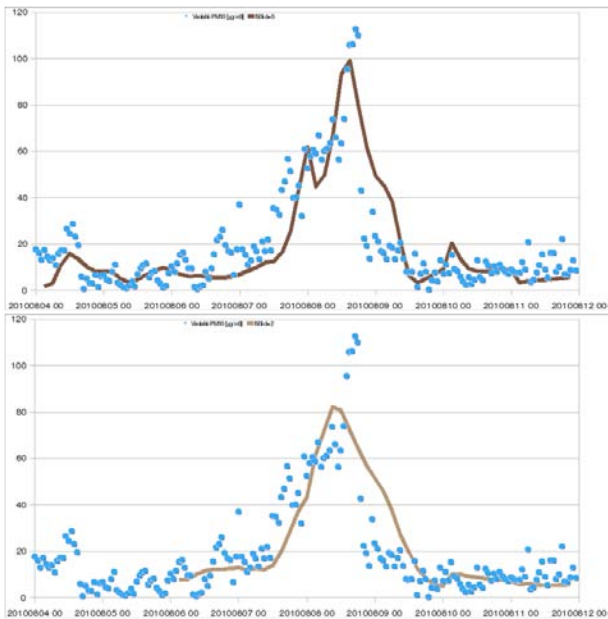


Figure 8. In-situ observations (symbols) and forecasts with 1 day (top line) and 3 days (bottom line) lead time of PM₁₀ in Virolahti, Finland, for 4–11 August 2010. (observations courtesy Finnish Meteorological Institute)

system as processed in MACC appears to allow characterising the fire type in near real time and adjusting the emission calculation dynamically. The global applicability of this in the MACC real time system is currently under investigation.

6. CONCLUSIONS

The MACC project is providing real time and retrospective services for the monitoring and forecasting of the global distribution of biomass burning and smoke plume spread. The fire monitoring is based on satellite-based fire observations. The plume monitoring and forecasting system is assimilating observations of AOD, CO, NO_x and other trace gases in addition to using emissions derived from the fire monitoring.

The fire emissions are calculated from a combination the GFED inventory with FRP observations for retrospective studies. For real time applications, MACC is running the first Global Fire Assimilation System (GFAS) based on FRP observations. It ingests fire products from the satellite-based MODIS, SEVIRI and GOES Imager instruments. The system is also unique in that it uses observations of no fire occurring to avoid ad hoc assumptions on the diurnal cycle of fires. Thus it is able to characterise the diurnal cycles of the observed fires. Observation gaps are filled with a data assimilation technique in the upcoming version.

The real time fire and smoke analyses over South America consistently record an increase of biomass burning

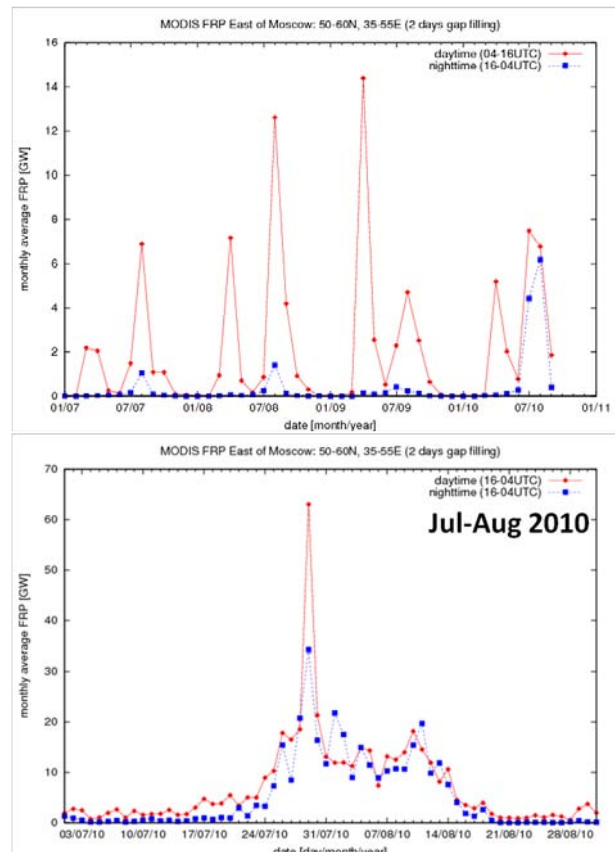


Figure 9. FRP observed during daytime (red) and nighttime (blue) east of Moscow. Monthly values are shown for 2007–2010 (top). Daily values are shown for July and August 2010 (bottom).

by a factor of about three for the biomass burning season 2010 when compared to the previous year. Like the comparable fire season in 2007, it coincides with a transition from El Niño to La Niña. This demonstrates the global monitoring capability with short response times of the MACC system.

During the catastrophic Russian fires in summer 2010, the MACC near real time system was able to forecast the resulting transgression of a European air quality threshold in Virolahti, Finland, with three days lead time. This proves the applicability of the global MACC systems for regional air quality applications, in addition to the regional MACC services. MACC's fire assimilation system is able to identify the fact that peaty soils were burning in Russia from the observed diurnal cycle of the fires. This has been shown to be the distinctive feature of this summer's fires that made them produce large amounts of smoke.

All MACC services are publicly available, see <http://www.gmes-atmosphere.eu/fire>.

ACKNOWLEDGMENTS

This research was supported by the EU Seventh Research Framework Programme (MACC project, contract number 218793).

REFERENCES

- [AM01] M.O. Andreae and P. Merlet. Emission of trace gases and aerosols from biomass burning. *Global Biogeochemical Cycles*, 15(4):955–966, 2001.
- [BMB⁺09] A. Benedetti, J.-J. Morcrette, O. Boucher, A. Dethof, R. J. Engelen, M. Fisher, H. Flentje, N. Huneus, L. Jones, J. W. Kaiser, et al. Aerosol analysis and forecast in the European Centre for Medium-Range Weather Forecasts Integrated Forecast System: 2. Data assimilation. *JGR*, 114(D13):D13205, 2009.
- [HET⁺08] A. Hollingsworth, R. J. Engelen, C. Textor, A. Benedetti, O. Boucher, F. Chevallier, A. Dethof, H. Elbern, H. Eskes, J. Flemming, C. Granier, J. W. Kaiser, J.-J. Morcrette, P. Rayner, V.-H. Peuch, L. Rouil, M. G. Schultz, A. J. Simmons, and "the GEMS Consortium". Toward a monitoring and forecasting system for atmospheric composition: The GEMS project. *Bulletin of the American Meteorological Society*, 89(8):1147–1164, 2008.
- [HKvdW⁺10] A. Heil, J.W. Kaiser, G.R. van der Werf, M.J. Wooster, M.G. Schultz, and H. Dernier van der Gon. Assessment of the real-time fire emissions (gfasv0) by macc. *Tech. Memo. 628*, 2010.
- [HSE⁺01] B. N. Holben, A. Smirnov, T. F. Eck, I. Slutsker, N. Abuhassan, W. W. Newcomb, J. S. Schafer, D. Tanre, B. Chatenet, and F. Lavenu. An emerging ground-based aerosol climatology: Aerosol optical depth from AERONET. *JGR*, 106(D11):12067–12097, 2001.
- [IK05] C. Ichoku and Y. J. Kaufman. A method to derive smoke emission rates from MODIS fire radiative energy measurements. *IEEE TGRS*, 43(11):2636–2649, 2005.
- [JGK⁺02] C. O. Justice, L. Giglio, S. Korontzi, J. Owens, J. T. Morisette, D. Roy, J. Descloitres, S. Alleaume, F. Petitcolin, and Y. Kaufman. The MODIS fire products. *RSE*, 83:244–262, 2002.
- [KFS⁺09] J.W. Kaiser, J. Flemming, M.G. Schultz, M. Suttie, and M.J. Wooster. The macc global fire assimilation system: First emission products (gfasv0). *ECMWF Tech. Memo. 596*, 2009.
- [KSF⁺09] J. W. Kaiser, M. Suttie, J. Flemming, J.-J. Morcrette, O. Boucher, and M.G. Schultz. Global real-time fire emission estimates based on space-borne fire radiative power observations. *AIP Conference Proceedings*, 1100:645–648, 2009.
- [KSG⁺06] J. W. Kaiser, M. G. Schultz, J. M. Gregoire, C. Textor, M. Sofiev, E. Bartholome, M. Leroy, R. J. Engelen, and A. Hollingsworth. Observation Requirements for Global Biomass Burning Emission Monitoring. In *Proceedings of the 2006 EUMETSAT Meteorological Satellite Conference*, 2006.
- [RW08] G. J. Roberts and M. J. Wooster. Fire detection and fire characterization over Africa using Meteosat SEVIRI. *IEEE TGRS*, 46(4):1200–1218, 2008.
- [vdWRG⁺06] G. R. van der Werf, J. T. Randerson, L. Giglio, G. J. Collatz, and P. S. Kasibhatla. Interannual variability in global biomass burning emissions from 1997 to 2004. *Atmos. Chem. Phys.*, 6(11):3423–3441, 2006.
- [vdWRG⁺10] G.R. van der Werf, J.T. Randerson, L. Giglio, G.J. Collatz, M. Mu, P.S. Kasibhatla, D.C. Morton, R.S. DeFries, Y. Jin, and T.T. van Leeuwen. Global fire emissions and the contribution of deforestation, savanna, forest, agricultural, and peat fires (1997–2009). *Atmos. Chem. Phys. Discuss*, 10:16153–16230, 2010.
- [WRPK05] M. J. Wooster, G. Roberts, G. L. W. Perry, and Y. J. Kaufman. Retrieval of biomass

combustion rates and totals from fire radiative power observations: FRP derivation and calibration relationships between biomass consumption and fire radiative energy release. *JGR*, 110, 2005.

- [XWRF10] W. Xu, MJ Wooster, G. Roberts, and P. Freeborn. New GOES imager algorithms for cloud and active fire detection and fire radiative power assessment across North, South and Central America. *Remote Sensing of Environment*, 2010.